

## 1 **C1 CAGE detects transcription start sites and enhancer activity at single-cell resolution**

2

3 Tsukasa Kouno<sup>1\*</sup>, Jonathan Moody<sup>1\*</sup>, Andrew Kwon<sup>1\*</sup>, Youtaro Shibayama<sup>1</sup>, Sachi Kato<sup>1</sup>, Yi  
4 Huang<sup>1,2</sup>, Michael Böttcher<sup>1</sup>, Efthymios Motakis<sup>1,3</sup>, Mickaël Mendez<sup>1,4</sup>, Jessica Severin<sup>1</sup>,  
5 Joachim Luginbühl<sup>1</sup>, Imad Abugessaisa<sup>1</sup>, Akira Hasegawa<sup>1</sup>, Satoshi Takizawa<sup>1</sup>, Takahiro  
6 Arakawa<sup>1</sup>, Masaaki Furuno<sup>1</sup>, Naveen Ramalingam<sup>5</sup>, Jay West<sup>5</sup>, Harukazu Suzuki<sup>1</sup>, Takeya  
7 Kasukawa<sup>1</sup>, Timo Lassmann<sup>1,6</sup>, Chung-Chau Hon<sup>1</sup>, Erik Arner<sup>1</sup>, Piero Carninci<sup>1</sup>, Charles  
8 Plessy<sup>1#</sup> and Jay W Shin<sup>1#</sup>

9

10 1 RIKEN Center for Integrative Medical Sciences (IMS), 1-7-22 Suehiro-cho, Tsurumi-ku,  
11 Yokohama, 230-0045 Japan

12 2 Present address: ACT Genomics Co., LTD., 3F., No.345, Xinhua 2nd Rd., Neihu Dist., Taipei  
13 City 114, Taiwan

14 3 Present address: Yong Loo Lin School of Medicine MD6, #08-01, 14 Medical Drive, National  
15 University of Singapore, Singapore 117599

16 4 Present address: Princess Margaret Cancer Research Tower 11-401, 101 College Street,  
17 Toronto, ON M5G 1L7 Canada

18 5 Single-Cell Research and Development, 7000 Shoreline Court, Suite 100, South San  
19 Francisco, California, USA 94080.

20 6 Present address: Telethon Kids Institute, The University of Western Australia, Subiaco,  
21 Australia

22

23 (\*) Authors contributed equally

24 (#) Corresponding authors: [plessy@riken.jp](mailto:plessy@riken.jp), [jay.shin@riken.jp](mailto:jay.shin@riken.jp)

25

## 26 **Abstract**

27 Single-cell transcriptomic profiling is a powerful tool to explore cellular heterogeneity. However,  
28 most of these methods focus on the 3'-end of polyadenylated transcripts and provide only a  
29 partial view of the transcriptome. We introduce C1 CAGE, a method for the detection of  
30 transcript 5'-ends with an original sample multiplexing strategy in the C1<sup>TM</sup> microfluidic system.  
31 We first quantified the performance of C1 CAGE and found it as accurate and sensitive as other  
32 methods in C1 system. We then used it to profile promoter and enhancer activities in the cellular  
33 response to TGF- $\beta$  of lung cancer cells and discovered subpopulations of cells differing in their  
34 response. We also describe enhancer RNA dynamics revealing transcriptional bursts in subsets  
35 of cells with transcripts arising from either strand within a single-cell in a mutually exclusive  
36 manner, which was validated using single molecule fluorescence in-situ hybridization.

## 37 Introduction

38 Single-cell transcriptomic profiling can be used to uncover the dynamics of cellular states and  
39 gene regulatory networks within a cell population(Trapnell, 2015; Wagner, Regev and Yosef,  
40 2016). Most available single-cell methods capture the 3'-end of transcripts and are unable to  
41 identify where transcription initiates. Instead, capturing the 5'-end of transcripts allows the  
42 identification of transcription start sites (TSS) and thus the inference of the activities of their  
43 regulatory elements. Cap analysis gene expression (CAGE), which captures the 5'-end of  
44 transcripts, is a powerful tool to identify TSS at single nucleotide resolution(Shiraki *et al.*, 2003;  
45 Carninci *et al.*, 2006). Using this technique, the FANTOM consortium has built an atlas of TSS  
46 across major human cell-types and tissues(Forrest *et al.*, 2014), analysis of which has led to the  
47 identification of promoters as well as enhancers in the human genome(Andersson *et al.*, 2014;  
48 Hon *et al.*, 2017). Enhancers have been implicated in a variety of biological processes(Lam *et*  
49 *al.*, 2014; Li, Notani and Rosenfeld, 2016), including the initial activation of responses to  
50 stimuli(Arner *et al.*, 2015) and chromatin remodeling for transcriptional activation(Mousavi *et al.*,  
51 2013). In addition, over 60% of the fine-mapped causal noncoding variants in autoimmune  
52 disease lay within immune-cell enhancers (Farh *et al.*, 2015), suggesting the relevance of  
53 enhancers in pathogenesis of complex diseases. Enhancers have been identified by the  
54 presence of balanced bidirectional transcription producing enhancer RNAs (eRNAs), which are  
55 generally short, unstable and non-polyadenylated (non-polyA)(Andersson *et al.*, 2014). Single  
56 molecule fluorescence *in situ* hybridization (smFISH) studies have suggested that eRNAs are  
57 induced with similar kinetics to their target mRNAs but that co-expression at individual alleles  
58 was infrequent(Rahman *et al.*, 2016). However, the majority of enhancer studies have been  
59 conducted using bulk populations of cells meaning that the dynamics of how multiple enhancers  
60 combine to influence gene expression remains unknown.

61  
62 The majority of single-cell transcriptomic profiling methods(Picelli, 2017) rely on oligo-dT priming  
63 during reverse transcription, which does not capture non-polyA RNAs transcripts (e.g. eRNAs).  
64 The recently developed RamDA-seq(Hayashi *et al.*, 2018) method uses random priming to  
65 capture the full-length non-polyA transcripts including eRNAs. However, this method is not  
66 strand-specific and unable to pinpoint transcript 5'-ends; thus, it cannot detect the  
67 bidirectionality of eRNA transcription and cannot confidently distinguish reads derived from the  
68 primary transcripts of their host gene (i.e. intronic eRNAs). Methods are typically implemented  
69 for a specific single-cell handling platform (e.g. microwell, microfluidics or droplet-based

70 platforms)(Picelli, 2017), because each platform imposes strong design constraints on the  
71 critical steps of cell lysis and nucleic acid handling. The proprietary C1<sup>TM</sup> Single-Cell Auto Prep  
72 System (Fluidigm) uses disposable integrated fluidic circuits (IFCs) and provides a registry of  
73 publicly available single-cell transcriptomics methods (Supplementary Table 1), which can be  
74 customized. Previously, we introduced nanoCAGE(Plessy *et al.*, 2010), a method requiring only  
75 nanograms of total RNA as start material, based on a template switch mechanism combined  
76 with random priming to capture the 5'-ends of transcripts independent of polyA tails in a strand-  
77 specific manner. Here we develop C1 CAGE, a modified version of nanoCAGE customized to  
78 the C1 system to capture the 5'-ends of transcripts at single-cell resolution.

79

80 Current single-cell methods are usually limited in the number of samples that can be multiplexed  
81 within the same run. Thus, experimental designs requiring multiple replicates and different  
82 conditions are prone to batch effects, confounding biological information with the technical  
83 variation of each experiment(Tung *et al.*, 2017). To mitigate batch effects, we took advantage of  
84 the transparency of the C1 system to encode multiple cells perturbation states in a single run by  
85 fluorescent labeling and imaging.

86

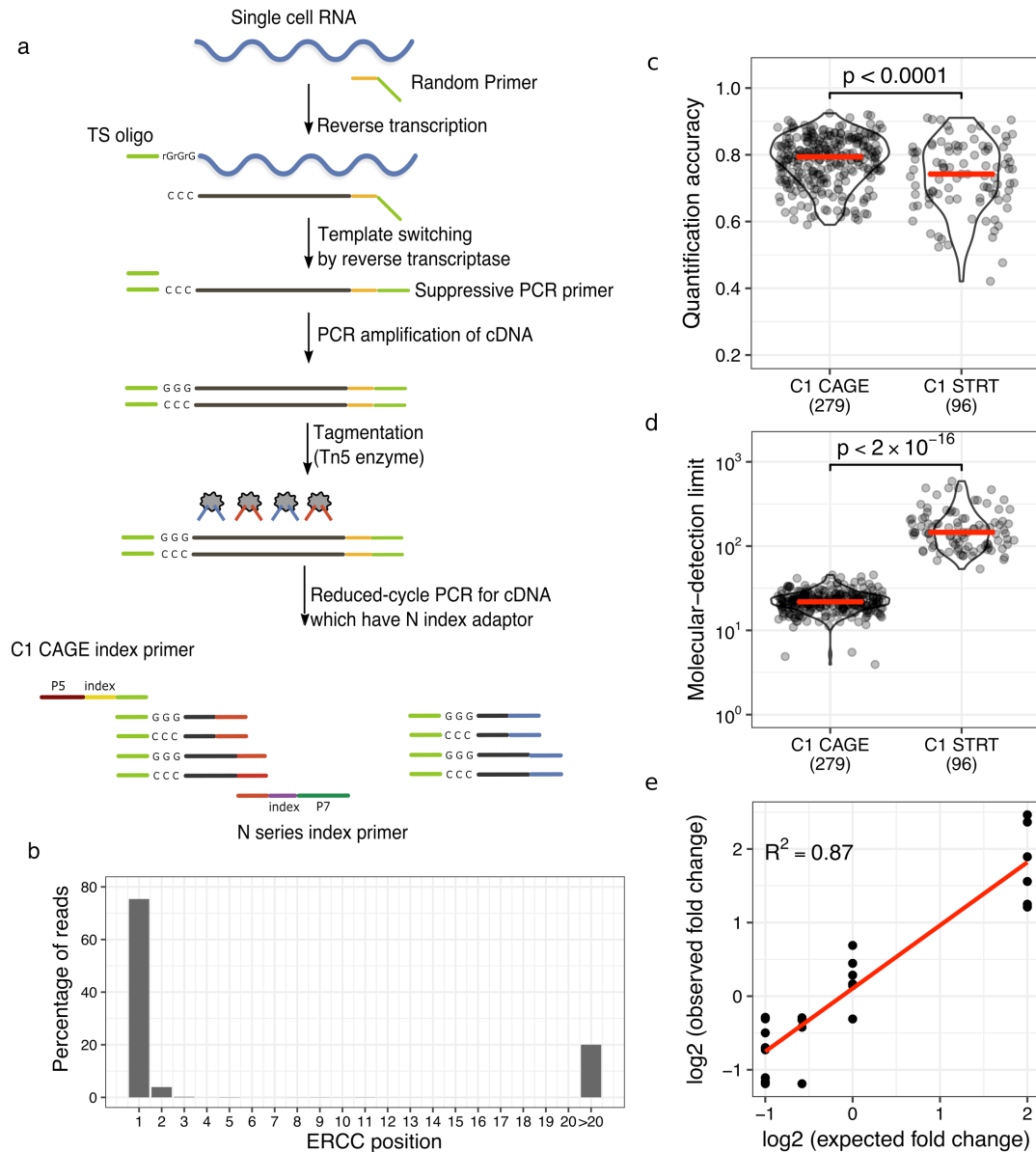
87 We apply this method to investigate the response to TGF- $\beta$  in A549 cells, an adenocarcinomic  
88 human alveolar basal epithelial cell line. TGF- $\beta$  signaling plays a key role in embryonic  
89 development, cancer progression, host tumor interactions and driving epithelial-to-mesenchymal  
90 transition (EMT)(Massagué, 2008; Ikushima and Miyazono, 2010). We examine the response to  
91 TGF- $\beta$  in A549 cells to uncover dynamically regulated promoters and enhancers at single-cell  
92 resolution. We observed an asynchronous cellular response to TGF- $\beta$  in sub-populations of  
93 cells. We also investigated the dynamics of enhancer transcription at single-cell resolution with  
94 validation by smFISH. Our results suggest transcriptional bursting of enhancers as reflected by  
95 high expression of eRNAs in a few cells. Also, while in pooled cells enhancers show  
96 bidirectional transcription, within single-cells transcription at enhancers is generally  
97 unidirectional—i.e. transcription on the two strands seems to be mutually exclusive.

## 98 Results

### 99 **Development of C1 CAGE**

100 We developed the C1 CAGE method, based on nanoCAGE(Plessy *et al.*, 2010), C1 STRT  
101 Seq(Islam *et al.*, 2014) and C1 RNA-seq(Wu *et al.*, 2014), implementing reverse transcription  
102 with random hexamers followed by template switching and pre-amplification (Figure 1a). The  
103 cDNA is tagged and the 5'-end of cDNA is specifically amplified by index PCR. The resulting  
104 library is sequenced from both ends, with the forward reads identifying the 5'-end of the  
105 transcript at single nucleotide resolution and the reverse read identifying downstream regions of  
106 the matching transcript.

107  
108 To assess the specificity of 5'-end capture, we prepared libraries of A549 cells in the presence  
109 of synthetic "spike-in" RNAs, a set of 92 exogenous control transcripts with defined abundances  
110 developed by the External RNA Controls Consortium (ERCC)(Munro *et al.*, 2014). We analyzed  
111 the positions of forward reads on these spike-ins and found that ~80% of their 5'-ends align to  
112 the first base (Figure 1b), supporting the specificity of 5'-end capture in C1 CAGE. Of the  
113 remaining reads, about half of them can be explained by "strand-invasion" events, which are  
114 artefacts arising from interruption of first strand synthesis due to complementarity with the  
115 template switching oligonucleotide and can be identified based on the upstream sequence of  
116 the read(Tang *et al.*, 2013). Next, we assessed the quantification accuracy and molecular  
117 detection limit(Svensson *et al.*, 2017). For quantification accuracy, measured as the Pearson  
118 correlation between the input spike-in amounts and the observed read counts, C1 CAGE  
119 displayed a median of 0.79, slightly higher (Welch Two Sample t-test, two-sided:  $t=4$ ,  $df=127.6$ ,  
120  $p < 0.0001$ ) than C1 STRT Seq (median of 0.74, Figure 1c). For detection limit, measured as  
121 the median number of spike-in molecules required to give a 50% chance of detection, C1 CAGE  
122 displayed a median of 22, which is significantly more sensitive (Welch Two Sample t-test, two-  
123 sided:  $t=-14$ ,  $df=94.2$ ,  $p < 2.2e-16$ ) compared with C1 STRT Seq (median of 146, Figure 1d).  
124 Finally, we assessed the ability of C1 CAGE to detect differential expression by comparing  
125 libraries prepared using two reference mixtures of spike-ins with fixed ratios of input amounts at  
126 4, 1, 2/3 and 1/2 fold difference. Fitting a linear model we find an R-squared value of  
127 87%(Figure 1e). These results demonstrate that C1 CAGE specifically captures the 5'-end of  
128 transcripts, has quantification accuracy and detection sensitivity comparable to other C1-system  
129 methods, and reliably detects differential expression with high accuracy.



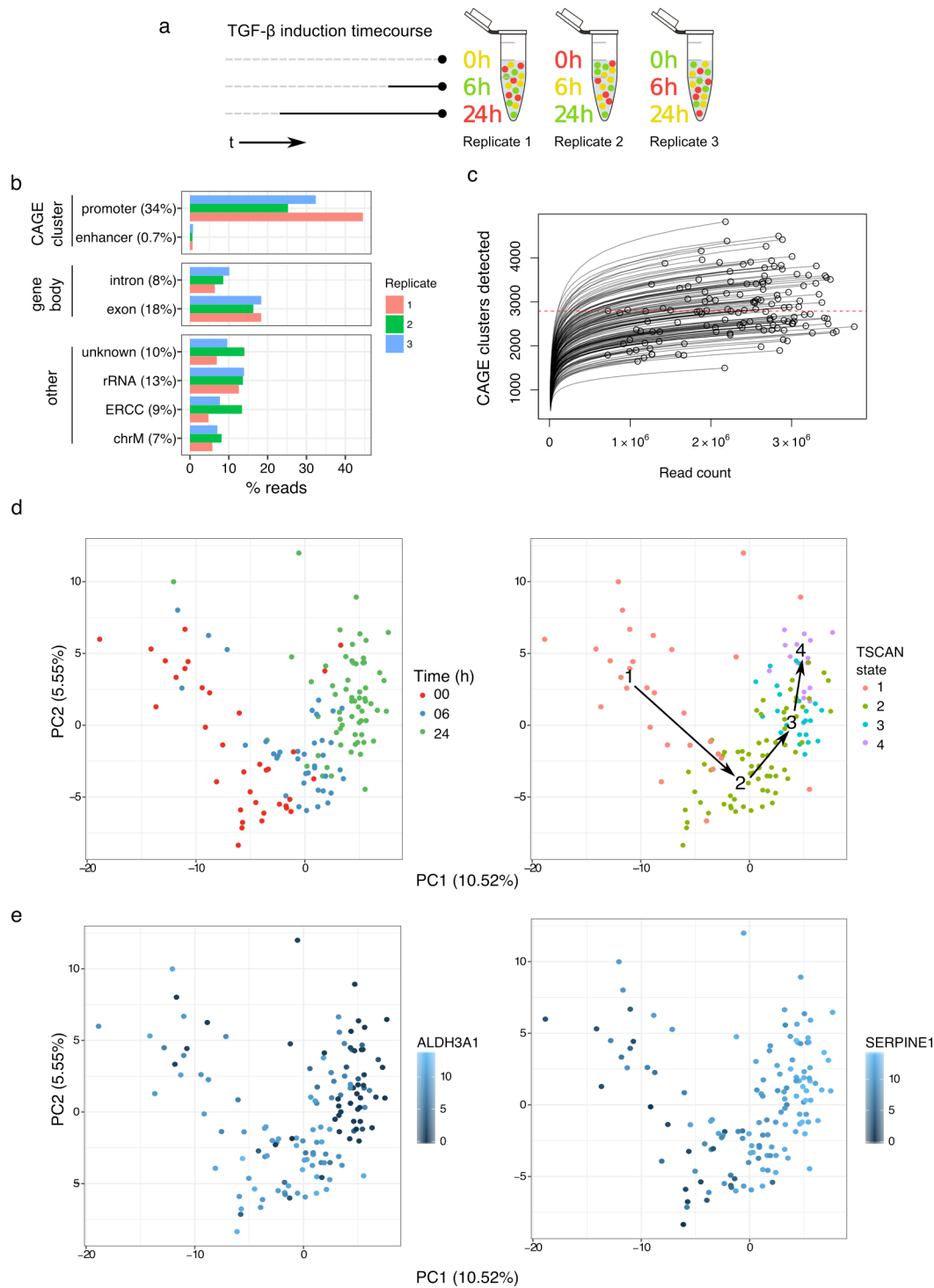
130

131 Figure 1: C1 CAGE method and performance

132 (a) Schematic of the C1 CAGE method. Tn5 enzymes are loaded with two different adaptors: N  
 133 (red) and S (blue). P5, P7: Illumina sequencing adaptors. (b) Percentage of reads aligning to the  
 134 5'-end of ERCC spike-ins by nucleotide position. (c, d) Comparison between C1 CAGE and C1  
 135 STRT Seq (data from doi:10.1038/nmeth.4220). Red bars show median values. p-values from  
 136 Welch two-sided Two Sample t-test shown. (c) Pearson correlation between expected and  
 137 observed ERCC spike-in molecules. (d) The number of ERCC spike-in molecules required for a  
 138 50 % chance of detection. (e) Observed and expected fold-change ratios between ERCC mix1  
 139 and mix2. Linear regression line (red) and R-squared value shown.

## 140 **Color multiplexing**

141 Taking advantage of the imaging capacities of the C1 system, we devised a strategy to  
142 multiplex samples within the same C1 CAGE replicate, by labelling cells with different Calcein  
143 AM dyes to encode sample information and monitor cell viability at the same time. Based on this  
144 approach, we multiplexed samples of A549 cells stimulated with TGF- $\beta$  in a time-course at three  
145 time-points (0, 6, and 24 h, in triplicates) by permuting the Calcein AM dyes for each time point  
146 in each replicate (Figure 2a). The three C1 CAGE replicates were sequenced to a median depth  
147 of 2.4 million raw read pairs per cell. Analyzing the genomic distribution of forward read 5'-ends  
148 per replicate, a mean of 34% and 0.7% of reads were aligned to promoter and enhancer CAGE  
149 clusters, respectively (Figure 2b). Subsampling analysis demonstrates the number of CAGE  
150 clusters detected in most single-cells are saturated at the current sequencing depths, with a  
151 median of 2,788 CAGE clusters detected per cell (Figure 2c). To demultiplex time points, we  
152 localized the cells in their capture chambers on the IFCs and quantified their fluorescence in the  
153 red and green channels, identifying 40, 41 and 70 cells for time points 0, 6 and 24 h,  
154 respectively. Following the scran pipeline(Lun, McCarthy and Marioni, 2016) we removed 15  
155 unreliable cells, arriving at the final set of 136 high quality cells. Initially, we observed a strong  
156 batch effect with principal components analysis (PCA), where cells cluster by replicate (Figure  
157 S1a). However, our experimental design ensured that each replicate contained cells for each  
158 time point, allowing us to correct for this batch effect using linear modelling. After batch  
159 correction cells were clustered by time points rather than by replicate (Figure S1b). After  
160 removing low abundance CAGE clusters, our final dataset detected 18,687 CAGE clusters,  
161 covering 9,809 GENCODE genes (Figure S2; annotation breakdown) and 826 FANTOM5  
162 enhancers. For comparison, we generated corresponding bulk CAGE data using the nAnT-  
163 iCAGE method(Murata *et al.*, 2014) for each sample (0, 6, and 24 h, in triplicates) sequenced to  
164 median a depth of 10.7M reads.



165

166 Figure 2: Multiplexing time course strategy

167 (a) Different color combinations of cells from each time point are added to each replicate. (b)

168 Forward read 5'-end counts by annotation category. Mean read percentage per category shown

169 in brackets. (c) Count of CAGE clusters within each cell after subsampling. Dashed red line at

170 median (2,788). (d) PCA of cells performed on variable subset of CAGE clusters, percentage of



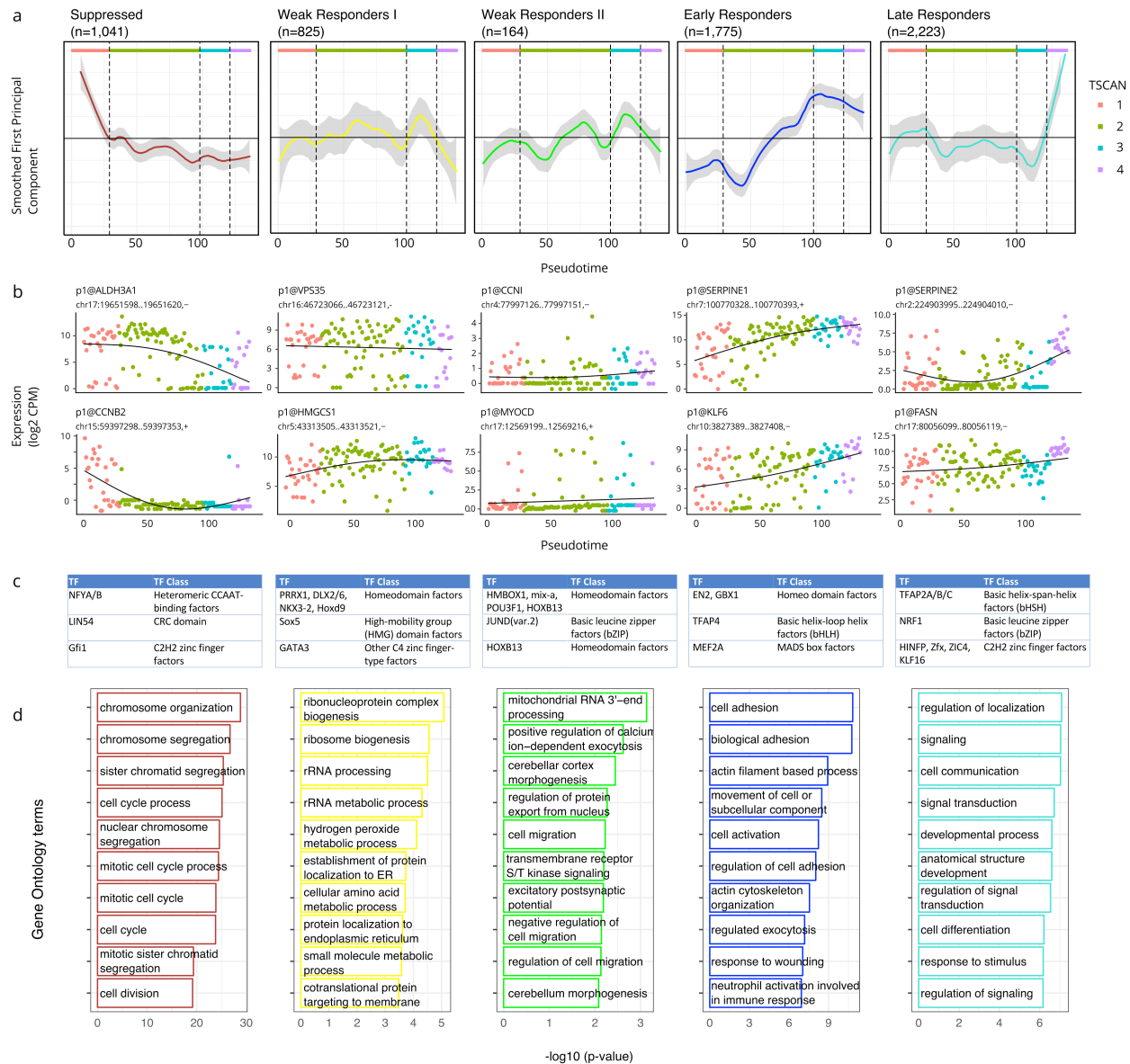
171 variance explained by components shown, cells colored by time point and TSCAN state. (e)  
172 PCA of cells performed on variable subset of CAGE clusters, percentage of variance explained  
173 by components shown, cells colored by expression values for the marker genes *ALDH3A1* and  
174 *SERPINE1* demonstrating that the dynamics of TGF- $\beta$  response are captured by the TSCAN  
175 states.

## 176 **Dynamic TSS regulation upon TGF- $\beta$ treatment**

177 To identify TSS that are dynamically regulated during TGF- $\beta$  treatment, we performed  
178 pseudotime analysis on a variable subset of CAGE clusters with TSCAN(Ji and Ji, 2016).  
179 TSCAN divided the pseudotime ordering into four distinct states, which showed considerable  
180 consistency with the time points, as seen by PCA (Figure 2d). We also confirmed the  
181 consistency of the TSCAN states by visualizing the expression levels of two highly variable  
182 CAGE clusters for known EMT marker genes, *ALDH3A1* and *SERPINE1*, which showed a clear  
183 shift in expression levels from 0 h to 24 h (Figure 2e). To understand the influence of the cell  
184 cycle on how TSCAN defined the states, we calculated G2M scores with the cyclone package  
185 using the pre-calculated data trained on human embryonic stem cells (hESCs)(Scialdone *et al.*,  
186 2015; Leng *et al.*, 2015). The clear separation of scores between states 1 and 2 points to the  
187 possibility that half (16/35) of 0 h cells were in proliferative states prior to TGF- $\beta$  stimulation  
188 (Figure 2d and Figure S3).

189  
190 To identify genes that are co-regulated across the TSCAN states, we performed Weighted Gene  
191 Co-Expression Network Analysis (WGCNA)(Langfelder and Horvath, 2008), correlating CAGE  
192 cluster expression levels across cells. We identified five co-expressed modules: Suppressed  
193 (n=1,041), Weak Responding I (n=825) & II (n=164), Early Responders (n=1,775), and Late  
194 Responders (n=2,223). We visualized their trajectories across the pseudotime using eigengene  
195 profiles to represent the average behavior and show two CAGE clusters from each module with  
196 eigengene correlation coefficient of at least 0.3 with p-value less than 0.1 (Figure 3a, b). The  
197 module labels were assigned based on these trajectory visualizations: Suppressed, Early and  
198 Late Responders represent those genes that undergo strong expression changes with TGF- $\beta$   
199 activation, whereas Weak Responding I and II represent those with little or no changes in their  
200 transcription.





201

202 Figure 3: WGCNA clusters of response to TGF $\beta$

203 (a) WGCNA results in 5 different modules, 3 of which show clear response behavior to TGF- $\beta$

204 (Suppressed, Early Responders, Late Responders). (b) Example CAGE peaks from each

205 module. (c) Top three enriched TF binding profiles in each module. (d) Functional analysis

206 using edgeR's implementation of Goseq. Top over-represented GO terms for biological

207 processes are shown.

208

209

210

211

212 To understand the biological contexts of these modules, we investigated the enrichment of  
213 transcription factor binding motifs (Mathelier *et al.*, 2016, Arenillas *et al.*, 2016) and Gene  
214 Ontology (GO) terms in each module. Examining motifs enriched in all modules against a  
215 randomly generated GC-matched background, we find that the ETS-related factors are most  
216 prominent, such as ETVn, ETSn, ELKn, FLI and NFYx factors (Figure S4). The ETS family of  
217 transcription factors is well defined to promote metastasis progression in EMT process(Ell and  
218 Kang, 2013).

219  
220 Examining each module individually against the combined background of all the other modules  
221 (Figure 3c, d) we observe the Suppressed Module enriched in GO terms related to DNA  
222 replication and the cell cycle. It has been reported that early after TGF- $\beta$  treatment, the  
223 expression of multiple genes that play key roles in regulating cell cycle progression are  
224 suppressed(Schneider, Tarantola and Janshoff, 2011). We observe suppressed expression of  
225 *CCNB2* known to interact with the TGF- $\beta$  pathway in promoting cell cycle arrest(Liu *et al.*, 1999)  
226 and of *ALDH3A1* known to affect cell growth in A549 cells(Moreb *et al.*, 2008). We also observe  
227 enriched motifs for the cell cycle regulators *LIN54* and *GFI1*(Basu *et al.*, 2009; Sadasivam and  
228 DeCaprio, 2013). CAGE clusters in the Suppressed module are more highly expressed in  
229 TSCAN state 1, which may represent cells which have not yet fully undergone TGF- $\beta$  induced  
230 G1 arrest as explained above.

231  
232 Within the Early Responders and Late Responders modules we observe canonical TGF- $\beta$   
233 response genes, including *KLF6* known to suppress growth through TGF- $\beta$   
234 transactivation(Botella *et al.*, 2009) and marker genes for EMT such as *SERPINE1* and *FASN*.  
235 TGF- $\beta$  is one of the key signal transduction pathways leading to EMT and several lines of  
236 evidence implicate increased TGF- $\beta$  signaling as a key effector of EMT in cancer progression  
237 and metastasis(Massagué, 2008; Ikushima and Miyazono, 2010; Heldin, Vanlandewijck and  
238 Moustakas, 2012). We observed upregulation of mesenchymal marker genes, with a clear  
239 increase in *Vimentin* (*VIM*) expression starting during TSCAN state 2, and expression of *N-*  
240 *cadherin* (*CDH2*) not detected until TSCAN state 2, and then expressed within a subset of  
241 cells(Figure S5).

242  
243 Within the Late Responders module we observe enrichment for TFAP2 family transcription  
244 factors (TFs) (Figure 3c), suggesting that they might play a role in the late response to TGF- $\beta$   
245 signaling. We examined their expression profiles in both the single-cell and bulk data, and found

246 *TFAP2C* to have a strong time-dependent expression profile in bulk data, and sporadic  
247 expression in TSCAN states 1 and 2 but not in the later states(Figure S6). *TFAP2C* is a known  
248 marker gene in breast cancer biology, its loss resulting in increased expression of mesenchymal  
249 markers associated with the transition from luminal to basal subtypes(Cyr *et al.*, 2015) and the  
250 direct repression of cell cycle regulator *CDKN1A*(Williams *et al.*, 2009; Wong *et al.*, 2012).

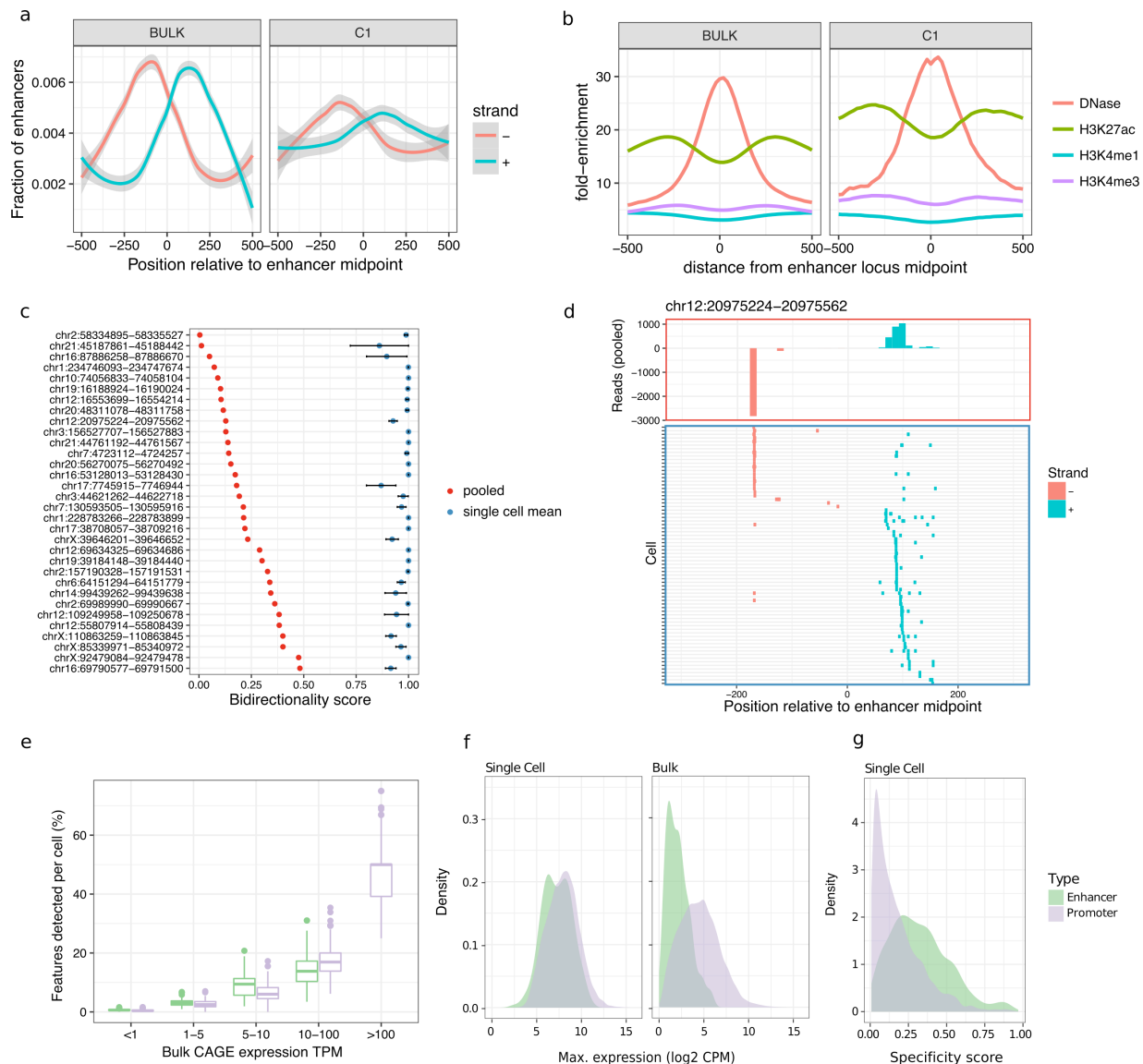
251  
252 Examining differences between the Early Responders and Late Responders modules, we find  
253 GO terms relating to cell adhesion enriched in Early Responders genes, and GO terms related  
254 to cell communication and signaling enriched in the Late Responders genes (Figure 3d).

255  
256 To further dissect the functional heterogeneity in response to TGF- $\beta$ , we revisited TSCAN states  
257 analysis and explored states 3 and 4 which we observe 24 h post stimulation (Figure 2d). To  
258 examine differences between the two states, we performed gene set enrichment analysis  
259 amongst CAGE clusters from the Early Responders and Late Responders modules with  
260 Camera(Wu and Smyth, 2012) and find a number of gene sets significantly upregulated in  
261 TSCAN state 4 including Epithelial to Mesenchymal transition (38 genes, FDR=0.003; full  
262 results in Supplementary Table 2). This suggests bi-phasic state in response to TGF- $\beta$  24 h post  
263 stimulation. Interestingly, a previous study implicated bi-phasic state with more severe  
264 morphological changes such as cell-to-cell contacts occurring from 10 to 30 h (Schneider,  
265 Tarantola and Janshoff, 2011). Thus, the additional states inferred from the pseudotime analysis  
266 reveal the asynchronous progression cells upon TGF- $\beta$  treatment, which would not have been  
267 possible with bulk analyses of the three time points.

## 268 **eRNA in C1 CAGE**

269 Next we asked whether C1 CAGE can detect the dynamic expression of eRNAs. We and others  
270 have reported that bidirectional transcription is associated with enhancer activity(Andersson *et al.*,  
271 2014). We observe a similar signature of bidirectional transcription at enhancers detected in  
272 pooled C1 CAGE and bulk CAGE data sets (Figure 4a), as well as a similar enrichment of  
273 DNase hypersensitivity and H3K27 acetylation, indicating that C1 CAGE unambiguously  
274 detected the transcription of eRNAs at these active enhancer regions (Figure 4b). To further  
275 examine the bidirectionality of eRNAs at a single-cell level, we selected enhancers with at least  
276 10 reads in at least 5 cells to filter for the most widely and strongly detected enhancers and  
277 avoid bias due to dropout. For each enhancer, we calculated a bidirectionality score in pooled  
278 single-cells ranging from 0 to 1, with 0 being perfectly balanced bidirectional and 1 being

279 perfectly unidirectional. Examining a set of enhancers (n=32) with balanced transcription, we  
 280 calculated their bidirectionality score within single-cells, where these enhancers were  
 281 unidirectionally transcribed (single-cell bidirectionality scores >0.9) (Figure 4c, shown in detail  
 282 for one enhancer in Figure 4d), indicating that simultaneous transcription of eRNAs from both  
 283 strands is generally not observed within single-cells.  
 284



285  
 286 **Figure 4: Enhancer analysis at single-cell resolution**  
 287 Comparison of enhancers detected by bulk CAGE and pooled C1 CAGE data (a) showing  
 288 bidirectional read profiles smoothed by generalized additive model and (b) epigenetic profiles.  
 289 (c) Bidirectionality analysis scores (0: equally bidirectional; 1: fully unidirectional) at selected  
 290 enhancers for pooled cells (red dots) and single-cells (blue dots: mean; black bars: standard

291 error). (d) Example locus on chromosome 12: read profile histogram (upper box), and read  
292 presence or absence in single-cells (lower box). (e, f, g) Comparison of enhancers and gene  
293 promoters in C1 CAGE and bulk CAGE: (e) Fraction of bulk features detected within each cell,  
294 stratified by bulk expression level, (f) Density plots of the maximum expression levels, (g)  
295 Specificity score distribution in single-cell data. Lower scores: broad expression (expressed in  
296 more cells); higher scores: more specific/enriched expression (fewer cells).

297

298 Although most enhancers were sporadically detected among single-cells, they were detected at  
299 a similar level to promoters in single-cells when controlling for expression level (Figure 4e). To  
300 assess if enhancers are generally lowly expressed among cells or if they are highly expressed  
301 in a subset of cells, we compared the distributions of the maximum expression levels of  
302 enhancers and promoters within single-cells and in the bulk data sets (Figure 4f). While the  
303 expression of enhancers is generally lower than that of promoters in the bulk data sets, they  
304 have similar distributions of expression levels within single-cells. To further evaluate the  
305 specificity of enhancer expression in single-cells, we devised a specificity score ranging from 0  
306 to 1, with 0 being ubiquitously expressed (i.e. broad expression in many cells), and 1 being  
307 specifically expressed (i.e. expression restricted to few cells). We found that enhancers show  
308 significantly higher specificity scores than promoters (Figure 4g; Kolmogorov-Smirnov test,  
309  $D=0.36562$ ,  $p\text{-value}<2.2e-16$ ). This suggests that enhancers behave similarly to promoters  
310 which are expressed in transcriptional bursts (Suter *et al.*, 2011; Bahar Halpern *et al.*, 2015) but  
311 have fewer numbers of cells where bursts of expression take place, which in turn are averaged  
312 out by the total population of cells used to obtain the bulk RNA profile.

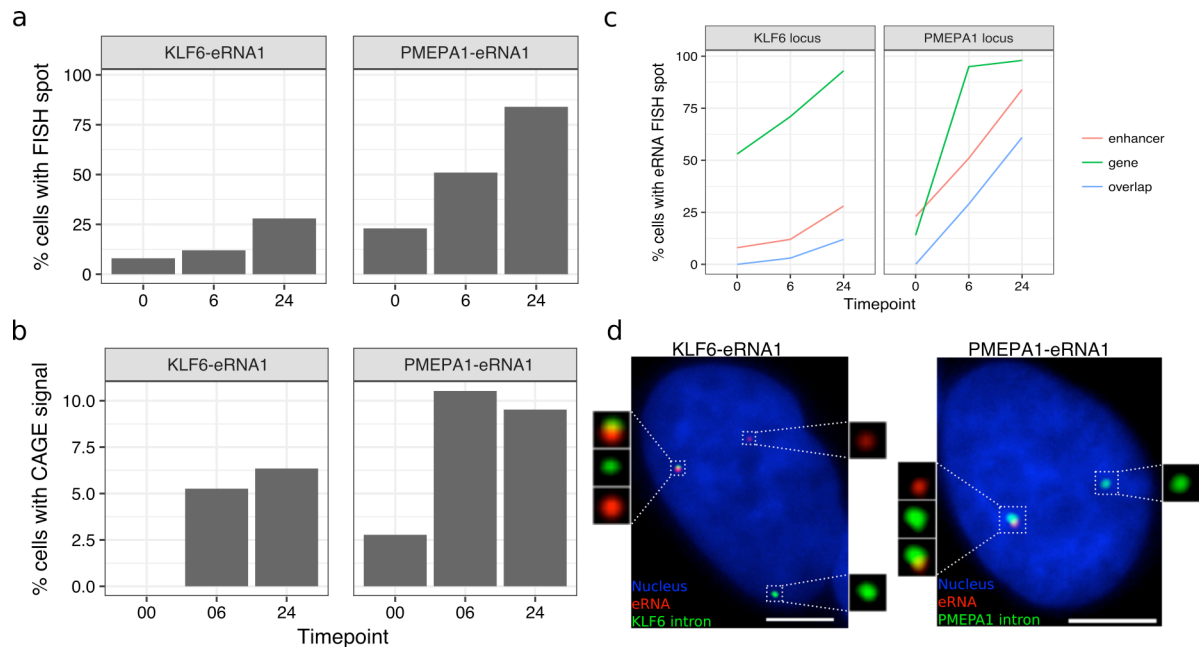
### 313 **FISH validation**

314 To validate the ability of C1 CAGE to detect eRNAs in single-cells, we used smFISH (Femino *et al.*  
315 *et al.*, 1998; Raj *et al.*, 2008) to visualize the expression of these transcripts through the TGF- $\beta$   
316 time course in A549 cells. We first selected intergenic enhancers, filtering out those that  
317 overlapped any known transcript models in GENCODEv25, and ranked them by their  
318 expression levels. We then searched for their proximal promoters within the same topologically  
319 associated domain (TAD) as the potential targets of these enhancers. We selected three  
320 enhancers, two of which displayed expression changes across the time-course (Figure S6, S7)  
321 and were adjacent to genes known to be involved in TGF- $\beta$  response, *KLF6* and *PMEPA1*  
322 (*KLF6*-eRNA1 at chr10:3929991-3930887 and *PMEPA1*-eRNA1 at chr20:56293544-56293843,

323 respectively), and a third enhancer (*PDK2*-eRNA1 at chr17:48105016-48105270) adjacent to  
324 *PDK2*.

325  
326 In line with previous reports (Rahman *et al.*, 2016; Shibayama, Fanucchi and Mhlanga, 2017),  
327 smFISH for eRNAs gave rise to punctate spots mainly restricted to the nuclei and always no  
328 greater than the copy number of the chromosome harboring the enhancer, suggesting that  
329 these eRNAs are expressed in low-copy-number and remain at or near their site of transcription.  
330 Targeting eRNAs on both strands with the same color, smFISH displayed expression profiles  
331 similar to C1 CAGE for the *KLF6*-eRNA1 and *PMEPA1*-eRNA1 enhancers that were  
332 upregulated in the C1 CAGE time-course data (Figure 5a, b). In contrast, *PDK2*-eRNA1, whose  
333 expression remained steady in smFISH, decreased in the number of cells with signal across the  
334 time course in C1 CAGE (Figure S8a).

335



336

337 Figure 5: Enhancer and promoter profiles in smFISH

338 (a, b) Proportion of cells with *KLF6*-eRNA1 and *PMEPA1*-eRNA1 detected by (a) FISH, (b) C1  
339 CAGE. (c) Proportion of cells with detected gene intron, enhancer locus and cells with spot  
340 overlap at the *KLF6* and *PMEPA1* loci. (d) Representative images showing gene intron and  
341 enhancer locus detection by FISH. Bar = 5  $\mu$ m. n=100 per time point.

342

343



344 For validation of our findings that eRNA were expressed unidirectionally within single-cells, we  
345 also targeted the + and – strands of the *KLF6*-eRNA1 and *PMEPA1*-eRNA1 eRNAs in separate  
346 colors. In agreement with the C1 CAGE data for these particular enhancers, the majority of the  
347 detected spots belonged to eRNAs from only one strand (Figure S8b). In nuclei where eRNAs  
348 from both strands were detected, spot co-localization was rare, confirming our suggestion that  
349 simultaneous bidirectional transcription of enhancers from single alleles is a rare event.

350

351 Next, we checked for the association of eRNAs with the transcription of nearby genes using  
352 smFISH. Visualization of nearby gene transcription was achieved by targeting only the intronic  
353 portion (i.e. nascent RNA). Colocalization of an enhancer RNA spot with a nascent RNA spot  
354 would suggest the presence of the enhancer RNA at the site of gene transcription, potentially  
355 implicating the enhancer's role in promoter activity. Interestingly, nascent transcription of nearby  
356 protein coding genes showed similar expression kinetics to the enhancers themselves indicated  
357 by increased co-expression of both the protein coding gene and the nearby eRNA in TGF- $\beta$   
358 stimulated cells (Figure 5c, d, S8c). For *KLF6*-eRNA1 and *PMEPA1*-eRNA1, we observed time-  
359 dependent increase in colocalization and in the number of nuclei with colocalized spots (Figure  
360 5c, d, S9c). In unstimulated cells displaying a basal level of expression of both enhancer and  
361 promoter, colocalization of spots could not be observed. This suggests a stimulus-dependent  
362 co-activation of enhancer and its association with the nearby promoter. However, a significant  
363 portion of transcription sites expressed no enhancer RNA. Possible reasons include a potential  
364 delayed interval between transcription events from an enhancer and promoter, during which  
365 most enhancer RNA is rapidly degraded. It is also possible that other nearby enhancers may  
366 exert their effect on a target promoter. In summary, smFISH could validate enhancer expression,  
367 including strand specificity, in single-cells as detected by C1 CAGE.

## 368 Discussion

369 We examined the response to TGF- $\beta$  in A549 cells to uncover dynamically regulated promoters  
370 and enhancers at single-cell resolution. We highlight enhancer dynamics at single-cell resolution  
371 and suggest transcriptional bursting of enhancers, and that while enhancers show bidirectional  
372 eRNA transcription in pooled cells, transcripts are generally mutually exclusive.

373

374 Among the eight publicly available transcriptome methods for the C1 platform (Supplemental  
375 table 1), only C1 CAGE provides strand-specific whole-transcriptome coverage: its detection of



376 5'-ends is independent from transcript length and polyadenylation owing to the use of random  
377 primers. To make the method more accessible, we used a commercially available tagmentation  
378 kit in which the transposase is loaded with two different adapters. This adaptation leads to half  
379 of the tagmentation products being lost in the process of library preparation. The use of custom  
380 loaded transposase, such as in C1 STRT Seq(Islam *et al.*, 2014), would allow reduction of the  
381 final PCR amplification by one cycle and enrich extracted reads in the sequencing library,  
382 however at the expense of not using standard reagents.

383

384 C1 CAGE has single-nucleotide resolution of transcript 5'-ends, as demonstrated by the data on  
385 ERCC spike-ins, where 80% of read one 5'-ends align to the first base. In this study, we did not  
386 use ERCC spike-ins for normalization of endogenous genes, preferring to use size factors  
387 computed from pools of cells(Lun, Bach and Marioni, 2016), as experimental noise due to spike-  
388 in preparation may be introduced(Svensson *et al.*, 2017). Notably, we could detect the ERCC  
389 spike-ins even if they are not capped. Nevertheless, C1 CAGE shows a preference for capped  
390 ends, as suggested by the fact that the C1 CAGE library contained only 13% reads from  
391 ribosomal RNAs. While this range of ribosomal RNA is acceptable, further reduction might be  
392 achieved through the use of pseudo-random primers(Arnaud *et al.*, 2016).

393

394 The template-switching oligonucleotides (TSOs) included Unique Molecular Identifier  
395 (UMIs)(Islam *et al.*, 2014), however we have not utilized them for molecular counting, because  
396 the TSOs carried over from the reverse-transcription could prime the subsequent PCR reaction  
397 while tolerating mismatches on the UMI sequence, thus causing a high level of mutation rate (as  
398 evidenced by the fact that most UMIs are seen only once). Nevertheless, PCR duplicates are  
399 partially removed from our data due to the use of paired-end sequencing, as our alignment  
400 workflow collapses the pairs that have exactly the same alignment coordinates. Further  
401 improvements of the C1 CAGE might address the mutation rate in UMIs. However, attempts to  
402 make the TSOs heat-labile by using full RNA composition have not been successful so far (CP  
403 and SK, personal communication).

404

405 Batch effect is a common problem in single-cell RNA-seq, and failing to account for this can  
406 lead to confounding biological interpretations. We introduced, for the first time, an image based  
407 approach to decode multiplex samples by using two colors of Calcein AM and their  
408 combinations. Moreover, the platform further allows the usage of a larger number of colors or  
409 alternatives to Calceins, such as MTT, ATP or MitoBright, which are generally used for live cell

410 monitoring. For instance, we previously used FUCCI fluorescent reporters to detect cell cycle  
411 phases(Böttcher *et al.*, 2016). Other potential applications could include the detection of  
412 cytoplasmic or nuclear localizations of fluorescent-labelled transcription factors, or cell division  
413 counting with fluorescent probes.

414  
415 Our cell cycle classification was performed using a model trained on data from H1 hESCs  
416 expressing the cell-cycle indicator FUCCI in the C1 system(Leng *et al.*, 2015). While training  
417 data from phased A549 single-cells would have been preferable, models trained on mouse ESC  
418 have also been applied to other cell types with accuracy(Scialdone *et al.*, 2015). However,  
419 because the hESC training data was obtained from a 3'-end capture protocol, it may contain  
420 different experimental biases that are distinct from our C1 CAGE method. Therefore, these  
421 results should be interpreted with caution, and we did not exclude cells based on this  
422 classification.

423  
424 The chemistry implemented in C1 CAGE—template switching, random priming, and interrogation  
425 of 5'-ends—revealed promoter and enhancer activities in lung adenocarcinoma cell line.  
426 Enhancers have previously been defined by a signature of balanced bidirectional transcription in  
427 bulk data(Andersson *et al.*, 2014). Here we suggest that this signature arises due to generally  
428 mutually exclusive transcription from each strand within single-cells. We also suggest for the  
429 first time that while eRNAs appear lowly expressed in bulk data, they can be expressed at  
430 similar levels to gene promoters within single-cells, although they are expressed in a more  
431 restricted subset of cells—i.e. displaying transcriptional bursting.

432  
433 Notably, C1 CAGE is not restricted to the use in the C1 platform. Indeed, some of the changes  
434 introduced in C1 CAGE are also available for bulk nanoCAGE libraries in our latest  
435 update(Poulain *et al.*, 2017). Moreover, the C1 CAGE chemistry might be applicable to profile  
436 large numbers of single-cells with droplet based single-cell capture methods. Droplet  
437 technologies are more robust to variations of the cell size, and have higher throughput, although  
438 they do not allow for the association of imaging. Five-prime-focused atlases will yield greater  
439 insights towards promoter and enhancer activities in various biological systems.

440

## 441 Online Methods

### 442 **Cell culture and TGF- $\beta$ stimulation**

443 A549 cells (ATCC CCL 185) were grown at 37 °C with 5 % CO<sub>2</sub> in DMEM (Wako, Lot:  
444 AWG7009) with 10 % fetal bovine serum (Nichirei Bioscience, Lot 1495557) and  
445 penicillin/streptomycin (Wako, Lot 168-23191). At 0 h, 10<sup>6</sup> cells were seeded in 10 cm dishes  
446 (TRP, Cat. num. 93100). At 24 h, the medium was replaced with DMEM without serum after 3  
447 times washing with PBS (Wako, Lot 045-29795). At 48 h, one third of the dishes were  
448 stimulated by treating with 5 ng/ml TGF- $\beta$  (R&D systems, USA, Accession #P01137). At 66 h,  
449 the second third was stimulated with the same treatment. At 72 h, cells for each treatment  
450 duration (0 h, 6 h 24 h) were collected and stained with combinations of Calcein AM and Calcein  
451 red-orange, (Thermo Fisher Scientific, L3224 and C34851). Transcriptome alignment of the C1  
452 positive controls against 79 reference genomes of Mycoplasma or Acholeplasma, including  
453 Mycoplasma hominis, confirmed the absence of contamination.

454

### 455 **Cell capture**

456 Calcein stained cells were captured in C1 Single-cell Auto Prep Integrated Fluidic Circuits (IFC)  
457 for mRNA Seq, designed for medium-sized (10 to 17  $\mu$ m) cells (Cat. Num. 100-5760), following  
458 manufacturer's instructions (PN 100-7168). In brief, 60  $\mu$ l of 2.5  $\times$  10<sup>5</sup> cell/ml and 40  $\mu$ l C1  
459 suspension buffer were mixed (all C1 reagents were from Fluidigm), and 20  $\mu$ l of this mix was  
460 loaded into a primed IFC, and processed the script "mRNA Seq: Cell load (1772x/1773x)"

461

### 462 **Imaging**

463 After loading, IFCs were imaged on INCell Analyzer 6000 (GE Healthcare). Calcein AM was  
464 excited at 488 nm and imaged with a FITC fluorescence filter (Semrock). For Calcein red-  
465 orange, excitation was at 561 nm (TexasRed; Semrock). Eleven focal planes per chamber and  
466 channel were acquired and manually curated to detect empty, dead, singlet, doublet or multiplet  
467 cells in the capture site. In case of single-plane imaging, we used the Cellomics platform like in  
468 Böttcher et al., 2016<sup>42</sup> (with a green filter (excitation bandwidth: 480-495 nm, emission  
469 bandwidth: 510-545 nm), and with a red filter (excitation bandwidth: 565-580 nm, emission  
470 bandwidth: 610-670 nm (Thermo Scientific)). Processed and raw single-cell images are  
471 available for download from [http://single-](http://single-cell.clst.riken.jp/riken_data/A549_TGF___summary_view.php)  
472 [cell.clst.riken.jp/riken\\_data/A549\\_TGF\\_\\_\\_summary\\_view.php](http://single-cell.clst.riken.jp/riken_data/A549_TGF___summary_view.php)

473

#### 474 **Lysis, reverse transcription and PCR for C1-CAGE**

475 Single-cell RNA extraction and cDNA amplification were performed on the C1 IFCs following the  
476 C1 CAGE procedure that we deposited in Fluidigm's Script Hub.  
477 (<https://www.fluidigm.com/c1openapp/scripthub/script/2015-07/c1-cage-1436761405138-3>). In  
478 brief, cells were loaded in lysis buffer (C1 loading reagent, 0.2 % Triton X, 15.2 U Recombinant  
479 Ribonuclease Inhibitor, 37.5 pmol reverse-transcription primer, DNA suspension buffer, ERCC  
480 RNA Spike-In Mix I or II (Thermo Fisher, 4456653) diluted either 20,000 times (protocol revision  
481 B) or 200 times (revision A)), and lysed by heat (72 °C 3 min, 4 °C 10 min, 25 °C 1 min). First-  
482 strand cDNAs were reverse transcribed (22 °C 10 min, 42 °C 90 min, 75 °C 15 min) in C1  
483 loading reagent, First Strand buffer, 0.24 pmol dithiothreitol, 15.4 nmol dNTP Mix, betaine, 24.8  
484 U Recombinant Ribonuclease Inhibitor, 175 pmol template-switching oligonucleotide, and 490 U  
485 SuperScript III. The cDNAs were amplified by PCR (95 °C 1 min, 30 cycles of 95 °C 15 s, 65 °C  
486 30 s and 68 °C 6 min, 72 °C 10 min) in a mixture containing C1 loading reagent, PCR water,  
487 Advantage2 PCR buffer (not SA), dNTP Mix (10 mM each), 24 pmol PCR primer, 50 ×  
488 Advantage2 Polymerase Mix. The PCR products (13 µl) were then harvested in a 96-well plate  
489 and quantified with the PicoGreen (Thermo Fisher, P11496) method following the instructions  
490 from Fluidigm's C1 mRNA-Seq protocol (PN 100-7168 I1). On-chip cDNA amplification with 30  
491 PCR cycles yielded 1.0 ng/µl in average from single cell. A subset of the samples were further  
492 controlled by size profiling on the Agilent Bioanalyzer with High Sensitivity DNA Chip.

493

#### 494 **Tagmentation reaction, index PCR and sequence**

495 Amplified cDNAs were diluted to approximately 0.2 ng/µl following the C1 mRNA-Seq protocol,  
496 fragmented and barcoded by "tagmentation" using the Nextera XT kit (Illumina, cat. num. FC-  
497 131-1096-RN) following the instructions from Fluidigm's C1 mRNA-Seq protocol (PN 100-7168  
498 I1), except that we used custom forward PCR primers (dir#501-508/N701-N712, Supplementary  
499 Table 3). The final purified library was quality-controlled on a High-Sensitivity DNA Chip and  
500 quantified with the KAPA Quantification Kit (Nippon Genetics). Nine pmol were sequenced and  
501 demultiplexed on Illumina HiSeq 2500 High output mode (50 nt paired end).

502

#### 503 **CAGE processing**

504 In forward read (Read 1) sequences, linkers were removed and unique molecular identifiers  
505 were extracted using TagDust2(Lassmann, 2015). Reverse read (Read 2) sequences were then  
506 filtered with the program syncpairs ([https://github.com/mmendez12/sync\\_paired\\_end\\_reads](https://github.com/mmendez12/sync_paired_end_reads)) to  
507 restore the pairing. The pairs were then filtered against the sequences of the human ribosomal

508 RNA locus (GenBank ID U13369.1), and linker oligonucleotides using TagDust2 v2.13 in paired-  
509 end mode. They were then aligned to the human genome version hg19 with Burrows Wheeler  
510 Aligner (BWA)'s "sampe" method(Li and Durbin, 2010) with a maximum insert size of 2,000,000.  
511 To map the reads on the ERCC spikes at a single nucleotide resolution, we prepared reference  
512 sequences of the T7 transcription of the ERCC plasmids, which are now available from the  
513 NIST's website ([https://www-](https://www-s.nist.gov/srmors/certificates/documents/SRM2374_putative_T7_products_NoPolyA_v1.fasta)  
514 [s.nist.gov/srmors/certificates/documents/SRM2374\\_putative\\_T7\\_products\\_NoPolyA\\_v1.fasta](https://www-s.nist.gov/srmors/certificates/documents/SRM2374_putative_T7_products_NoPolyA_v1.fasta))  
515 (many RNA-seq studies previously published aligned their reads only to the sequence of the  
516 plasmid inserts, which lack transcribed linker sequences, which are essential for aligning CAGE  
517 reads precisely to the 5' ends). The properly aligned pairs were then converted to BED12 format  
518 with the program `pairedBamToBed12` ([https://github.com/Population-](https://github.com/Population-Transcriptomics/pairedBamToBed12)  
519 [Transcriptomics/pairedBamToBed12](https://github.com/Population-Transcriptomics/pairedBamToBed12)) with the option "-extraG", and assembled in CAGEscan  
520 fragments with the program `umicountFP` (<https://github.com/mmendez12/umicount/>). This  
521 workflow was implemented in the Moirai system (PMID:24884663) and a prototype implemented  
522 in a Jupyter notebook is available on GitHub ([https://github.com/Population-Transcriptomics/C1-](https://github.com/Population-Transcriptomics/C1-CAGE-preview/blob/master/OP-WORKFLOW-CAGEscan-short-reads-v2.0.ipynb)  
523 [CAGE-preview/blob/master/OP-WORKFLOW-CAGEscan-short-reads-v2.0.ipynb](https://github.com/Population-Transcriptomics/C1-CAGE-preview/blob/master/OP-WORKFLOW-CAGEscan-short-reads-v2.0.ipynb)). The 5' ends  
524 of the CAGEscan fragments represent TSS in the sense of Sequence Ontology's term  
525 SO:0000315 ("The first base where RNA polymerase begins to synthesize the RNA transcript").

526

## 527 **Bulk CAGE**

528 Bulk CAGE data was generated by nAnt-iCAGE method(Murata *et al.*, 2014). Briefly, 5 µg of  
529 total RNA prepared from remaining A549 cells after C1 loading. cDNA was reverse transcribed  
530 using SuperScript III reverse transcriptase, biotinylated and cap trapped to capture 5' completed  
531 cDNAs. Each cDNAs were barcoded and purified. Libraries were sequenced on Illumina HiSeq  
532 2500 High output mode (50 nt single read).

533

## 534 **Image curation and time point demultiplexing**

535 We used the Bioconductor package CONFESS (LOW D and MOTAKIS E (2017). *CONFESS:*  
536 *Cell OrderiNg by FluorEScence Signal*. R package version 1.6.0) to detect the cells present in  
537 the capture chambers, and quantify the fluorescence in the Green and Red channels. In  
538 addition, two curators visually screened the images to confirm the presence of cells, and to  
539 detect doublets when focal stacks were available. The final annotation reflects the consensus of  
540 the three curations. The results were then cross-checked with other quality control parameters,  
541 in particular the amount of cDNAs yielded by the C1 runs, and the fraction of spikes and

542 ribosomal RNA in the libraries. In case of conflicting results, chamber images were re-inspected  
543 and re-annotated, if necessary.

544

### 545 **ERCC spike-in analysis**

546 Accuracy and molecular detection limits were calculated as in Svensson 2017(Svensson *et al.*,  
547 2017): The amount of input spike-in molecules for each spike, for each sample, in each  
548 experiment was calculated from the final concentration of ERCC spike-in mix in the sample. The  
549 calculation of the accuracy of an individual sample was determined with the Pearson correlation  
550 between input concentration of the spike-ins and the measured expression values. Molecular  
551 detection limit was calculated using the R function glm from the stats package.

552

### 553 **Read Annotation**

554 The annotation used combined FANTOM5 robust cage clusters for promoters  
555 ([http://fantom.gsc.riken.jp/5/datafiles/latest/extra/CAGE\\_peaks/](http://fantom.gsc.riken.jp/5/datafiles/latest/extra/CAGE_peaks/)) and enhancers  
556 (<http://fantom.gsc.riken.jp/5/datafiles/latest/extra/Enhancers/>). Promoter clusters were  
557 subtracted from enhancer clusters and annotated to their nearest GENCODEv25 within 500 bp  
558 where possible. A mask was added to remove rRNA, tRNA, small RNAs, unannotated  
559 promoters.

560

### 561 **Data Processing**

562 After removing low quality cells and multiple single cells captured sites based on imaging data  
563 (SCPortalen)(Abugessaisa *et al.*, 2018), the CAGE reads from the remaining 151 cells that  
564 overlapped the annotation CAGE clusters were summed together to create the raw counts  
565 matrix. This matrix was processed with the scran package(Lun, McCarthy and Marioni, 2016)  
566 version 1.6.6 in R 3.4.3 for quality control, filtering and normalization. Following the guideline  
567 suggested by the authors of scran, we first removed from our analysis 15 cells with 1) library  
568 sizes or feature sizes 3 median absolute deviations (MADs) below their median, or 2)  
569 mitochondrial proportion or spike proportion 3 MADs above their median, leaving us with 136  
570 cells. All the cells that were dropped due to high spike proportion also had low library sizes and  
571 feature counts, whereas this was not necessarily true for those that were dropped due to high  
572 mitochondrial proportion. 14 out of the 15 removed cells were from the same C1 run (library 2),  
573 but there was no noticeable bias towards any particular time point (5, 3, 7 cells from 0h, 6 h, 24  
574 h, respectively). We calculated the cell cycle phase scores using the cyclone method(Scialdone  
575 *et al.*, 2015) for each cell. We filtered out low abundance features that were expressed in less



576 than 2 cells or average counts of less than 0.3, leaving us with 18,687 features, of which 826  
577 are FANTOM5 enhancers. These features were normalized with size factors calculated based  
578 on clusters of cells with minimum size of 30. We then performed mean-variance trend fitting  
579 using the whole endogenous feature set, building the sample replicate and Calcein staining  
580 variables into the model. We normalized the expression scores to correct for differences of  
581 sequencing depth, using a pooling-deconvolution approach(Lun, Bach and Marioni, 2016). We  
582 then detrended the data for possible C1 run and Calcein color effects. Lastly, we denoised the  
583 data by removing low-rank principal components. To produce the final normalized expression  
584 levels for downstream analyses, we reduced the technical noise using scran's denoisePCA  
585 function based on the fitted data, then performed batch effect removal with the replicate and the  
586 Calcein stain as the covariates using limma package's removeBatchEffect function. We selected  
587 high variance CAGE clusters (HVCs) as those with biological variation above the 75% quantile  
588 and false discovery rate less than 0.05 after decomposing the total variance for each gene into  
589 its biological and technical components using trendVar (scran). We also calculated the pairwise  
590 correlations among the HVCs and marked those with FDR greater than 0.05 as significantly  
591 correlating HVGs.

592  
593 To create the pseudotime ordering with TSCAN (version 1.16.0), we selected the input feature  
594 set as the union of the significantly correlating HVCs, the top 100 HVCs and SC3(Kiselev *et al.*,  
595 2017) defined marker genes, totaling 290 CAGE clusters.

596

### 597 **WGCNA**

598 WGCNA version 1.61 was used, with cut height detection threshold of 0.995, minimum module  
599 size of 100, signed network type, and merge cut height of 0.25. To reduce noise, we restricted  
600 ourselves to those features with mean expression greater than the median of the mean  
601 expression across all samples, and biological variation greater than the median. Also, to avoid  
602 having the same gene appearing in multiple clusters due to different promoters of the same  
603 gene being assigned as such, we only included the major promoter (highest sum of normalized  
604 expression across all samples) in the input set, which left us with 6,028 CAGE clusters as the  
605 input set.

606

### 607 **Motif analysis**

608 Motif analysis was performed using CAGED-oPOSSUM, which employs two separate scoring  
609 systems based on JASPAR 2016 transcription factor binding profiles, searching 500bp either



610 side of CAGE clusters: 1) Z-scores, which counts the total number of a given motif found in the  
611 input set, and 2) Fisher score, which counts the number of input regions with the given motif.  
612 JASPAR motifs with information content greater than 8 bits were searched.

613

#### 614 **Functional analysis**

615 To see if we could identify any functional characteristics of the genes in each module, we  
616 performed a test of gene ontology term over-representation test using the edgeR's goana  
617 function, which is an implementation of GOseq(Young *et al.*, 2010). For input, we included those  
618 CAGE clusters that showed correlation coefficient of greater than 0.2 with p-value less than 0.1  
619 with each module's eigengene.

620

621 Camera gene set enrichment analysis(Wu and Smyth, 2012) was performed testing for  
622 differential expression between TSCAN states 3 and 4. For the input expression table, we  
623 selected the CAGE clusters that were included in the WGCNA analysis and were annotated with  
624 Entrezgene IDs. For the test set, we selected those CAGE clusters that showed correlation  
625 coefficient of greater than 0.2 with p-value less than 0.1 their module's eigengene from the Early  
626 Responders and Late Responders modules. MSigDB Hallmark gene sets were used.(Liberzon  
627 *et al.*, 2015)

628

#### 629 **TADs**

630 Out of 826 enhancers, 692 could be assigned to a topological association domain (TAD)  
631 identified in A549 cells from ENCODE Dataset GSE105600

632

#### 633 **FISH**

634 enhancer RNA lengths were estimated from the ENCODE A549 RNA-seq signal(Dunham *et al.*,  
635 2012). We designed oligonucleotide probes consisting of 20 nt targeting sequence using the  
636 Stellaris Probe Designer (Biosearch Tech). These sequences were flanked on both ends by 30  
637 nt "readout sequence" serving as annealing sites for secondary probes that are labeled with a  
638 fluorescent dye(Chen *et al.*, 2015). For each set of probes, all flanking sequences were identical,  
639 both on the 5' and 3' ends (Probes listed in Supplementary Table 4). Positive strand eRNA,  
640 negative strand eRNA and introns from each locus were assigned different flanking sequences  
641 to allow multiplexing. Secondary probes were labeled with either Atto 647 or Cy3 on the 3' end.  
642 All probe sequences are listed in supplementary table 4. Briefly, cells were seeded onto  
643 coverslips overnight and were fixed in 4% formaldehyde in PBS for 10 min at room temperature.

644 After fixation, the coverslips were treated twice with ice-cold 0.1% sodium borohydride for 5 min  
645 at 4°C. Following three washes in PBS, the coverslips were treated with 0.5% Triton X-100 in  
646 PBS for 10 min at room temperature to permeabilize the cells. The coverslips were washed  
647 three times in PBS and treated with 70% formamide in 2x SSC for 10 min at room temperature,  
648 followed by two washes in ice-cold PBS and another wash in ice-cold 2x SSC. The coverslips  
649 were stored at 4°C for no longer than a few hours prior to hybridization. For hybridization,  
650 coverslips were incubated in hybridization buffer containing 252 nM primary probes overnight at  
651 37°C inside a humid chamber. Hybridization buffer consisted of 10% formamide, 10% dextran  
652 sulfate, 2X SSC, 1µg/µl yeast tRNA, 2mM vanadyl ribonucleoside complex, 0.02% BSA. To  
653 remove excess probe, coverslips were washed twice in wash buffer made of 30% formamide,  
654 2x SSC, 0.1% Triton X-100 for 30 min at room temperature and rinsed once in 2x SSC. For  
655 hybridization with secondary probes labeled with fluorescent dyes, coverslips were incubated in  
656 minimal hybridization buffer (10% formamide, 10% dextran sulfate, 2x SSC) containing 30 nM  
657 secondary probes for 3 h at 37°C inside a humid chamber. Coverslips were again washed twice  
658 in wash buffer for 30 min at room temperature and rinsed once in 2x SSC. Coverslips were  
659 mounted on glass slides using ProLong Gold Antifade Mountant with DAPI (Invitrogen). Imaging  
660 was done on a DeltaVision Elite microscope (GE) equipped with a sCMOS camera. Image  
661 processing and analysis were done using FIJI.

662

### 663 **Enhancer Analysis**

664 For bidirectionality and epigenetic marks analysis a set of enhancers was selected overlapping  
665 ReMap(Chèneby *et al.*, 2018) EP300 A549 binding sites. DNase, H3K27ac, H3K4me1 and  
666 H3K4me3 bigwig files were downloaded from the NIH roadmap epigenomics project(Roadmap  
667 Epigenomics Consortium *et al.*, 2015) and processed with computeMatrix scale-regions from  
668 the deeptools package(Ramírez *et al.*, 2016) for enhancer regions. Bidirectional enhancers  
669 were selected with at least 10 reads in at least 5 cells and a bidirectionality statistic was  
670 calculated as:  $\text{abs}(plus\ strand\ reads - minus\ strand\ reads) / \text{sum}(reads)$  ranging from 0 to 1 with  
671 0 being equally bidirectional and 1 being fully unidirectional. 32 enhancers were selected with  
672 absolute score  $\leq 0.5$ . This score was then calculated within each individual cell for these  
673 enhancers. The specificity score to indicate how broadly/specifically TSS were expressed we  
674 calculated:  $Enrichment = \text{Max.Expression} / \sum(\text{Expression across all samples})$ .

675

676

677

678 **Data Availability.**

679 C1 CAGE sequence data from this study have been submitted to DDBJ (Project ID:  
680 PRJDB5282, Sample ID: SAMD00066188 - SAMD00066475). Alignments were uploaded to the  
681 ZENBU genome browser (Severin et al, 2014, PMID 24727769) and a default view is available  
682 at <http://fantom.gsc.riken.jp/zenbu/gLyphs/#config=NMT9yTLnH59gIVssI9WRfD>. In these two  
683 submissions the libraries numbered 1, 2 and 3 in this manuscript are numbered 4, 5 and 6,  
684 respectively, for historical reasons.

685 **Code Availability.**

686 Code used in this study is available at [https://github.com/Population-Transcriptomics/C1-CAGE-](https://github.com/Population-Transcriptomics/C1-CAGE-manuscript)  
687 manuscript

688 **Acknowledgements**

689 This work was supported by a Research Grant from the Japanese Ministry of Education, Culture,  
690 Sports, Science and Technology (MEXT) to the RIKEN Center for Life Science Technologies.  
691 The authors wish to acknowledge RIKEN GeNAS for the sequencing of the libraries, and Fumi  
692 Hori for data deposition to DDBJ.

693  
694 **Author Contributions**

695 Conceptualization: TL, EA, CP, JWS  
696 Ideas; formulation or evolution of overarching research goals and aims.

697  
698 Data curation: TKo, AK, YH, MM, JSe, IA, CP  
699 Management activities to annotate (produce metadata), scrub data and maintain research data  
700 (including software code, where it is necessary for interpreting the data itself) for initial use and  
701 later re-use.  
702

703  
704 Formal analysis: JM, AK, YH, EM  
705 Application of statistical, mathematical, computational, or other formal techniques to analyze or  
706 synthesize study data.  
707

708 Funding acquisition: PC, JWS  
709 Acquisition of the financial support for the project leading to this publication.  
710

711 Investigation: TKo, YS, SK, MB  
712 Conducting a research and investigation process, specifically performing the experiments, or  
713 data/evidence collection.  
714

715 Methodology: TKo, YS, SK, JL, CP, JWS

716 Development or design of methodology; creation of models.  
717  
718 Project administration: PC, CP, JWS  
719 Management and coordination responsibility for the research activity planning and execution.  
720  
721 Resources: ST, TA, MF, NR, JW, HS  
722 Provision of study materials, reagents, materials, patients, laboratory samples, animals,  
723 instrumentation, computing resources, or other analysis tools.  
724  
725 Software: JM, AK, MB, MM, JSe, IA, AH, TL, CP  
726 Programming, software development, designing computer programs implementation of the  
727 computer code and supporting algorithms, testing of existing code components.  
728  
729 Supervision: HS, TKa, TL, CCH, EA, CP, JWS  
730 Oversight and leadership responsibility for the research activity planning and execution,  
731 including mentorship external to the core team.  
732  
733 Validation: TKo, YS  
734 Verification, whether as a part of the activity or separate, of the overall replication/reproducibility  
735 of results/experiments and other research outputs.  
736  
737 Visualization: JM, AK, IA, CP  
738 Preparation, creation and/or presentation of the published work, specifically visualization/data  
739 presentation.  
740  
741 Writing – original draft: TKo, JM, AK, YS, EA, CP, JWS  
742 Preparation, creation and/or presentation of the published work, specifically writing the initial  
743 draft (including substantive translation).  
744  
745 Writing – review & editing: JM, CP, JWS  
746 Preparation, creation and/or presentation of the published work by those from the original  
747 research group, specifically critical review, commentary or revision– including pre- or post-  
748 publication stages.  
749

750

## 751 Conflict of interest

752

753 Dr. Ramalingam is an employee and stockholder of Fluidigm Corporation.

754

## 755 References

- 756 Abugessaisa, I. *et al.* (2018) 'SCPortalen: human and mouse single-cell centric database.',  
757 *Nucleic acids research*, 46(D1), pp. D781–D787. doi: 10.1093/nar/gkx949.
- 758 Andersson, R. *et al.* (2014) 'An atlas of active enhancers across human cell types and tissues',  
759 *Nature*, 507(7493), pp. 455–461. doi: 10.1038/nature12787.
- 760 Arenillas, D. J. *et al.* (2016) 'CAGEd-oPOSSUM: motif enrichment analysis from CAGE-derived  
761 TSSs.', *Bioinformatics (Oxford, England)*, 32(18), pp. 2858–60. doi:  
762 10.1093/bioinformatics/btw337.
- 763 Arnaud, O. *et al.* (2016) 'Targeted reduction of highly abundant transcripts using pseudo-  
764 random primers', *BioTechniques*, 60(4), pp. 169–174. doi: 10.2144/000114400.
- 765 Arner, E. *et al.* (2015) 'Transcribed enhancers lead waves of coordinated transcription in  
766 transitioning mammalian cells.', *Science (New York, N.Y.)*, 347(6225), pp. 1010–4. doi:  
767 10.1126/science.1259418.
- 768 Bahar Halpern, K. *et al.* (2015) 'Bursty gene expression in the intact mammalian liver.',  
769 *Molecular cell*, 58(1), pp. 147–56. doi: 10.1016/j.molcel.2015.01.027.
- 770 Basu, S. *et al.* (2009) 'Gfi-1 represses CDKN2B encoding p15INK4B through interaction with  
771 Miz-1', *Proceedings of the National Academy of Sciences*, 106(5), pp. 1433–1438. doi:  
772 10.1073/pnas.0804863106.
- 773 Botella, L. M. *et al.* (2009) 'TGF-beta regulates the expression of transcription factor KLF6 and  
774 its splice variants and promotes co-operative transactivation of common target genes through a  
775 Smad3-Sp1-KLF6 interaction.', *The Biochemical journal*, 419(2), pp. 485–95. doi:  
776 10.1042/BJ20081434.
- 777 Böttcher, M. *et al.* (2016) 'Single-cell transcriptomes of fluorescent, ubiquitination-based cell  
778 cycle indicator cells', *bioRxiv*. Available at:  
779 <http://biorxiv.org/content/early/2016/12/15/088500.abstract>.
- 780 Carninci, P. *et al.* (2006) 'Genome-wide analysis of mammalian promoter architecture and  
781 evolution.', *Nature genetics*, 38(6), pp. 626–35. doi: 10.1038/ng1789.
- 782 Chen, K. H. *et al.* (2015) 'Spatially resolved, highly multiplexed RNA profiling in single cells.',  
783 *Science (New York, N.Y.)*, 348(6233), p. aaa6090. doi: 10.1126/science.aaa6090.
- 784 Chèneby, J. *et al.* (2018) 'ReMap 2018: an updated atlas of regulatory regions from an  
785 integrative analysis of DNA-binding ChIP-seq experiments.', *Nucleic acids research*, 46(D1), pp.  
786 D267–D275. doi: 10.1093/nar/gkx1092.
- 787 Cyr, A. R. *et al.* (2015) 'TFAP2C governs the luminal epithelial phenotype in mammary  
788 development and carcinogenesis', *Oncogene*, 34(4), pp. 436–444. doi: 10.1038/onc.2013.569.

- 789 Dunham, I. *et al.* (2012) 'An integrated encyclopedia of DNA elements in the human genome',  
790 *Nature*, 489(7414), pp. 57–74. doi: 10.1038/nature11247.
- 791 Ell, B. and Kang, Y. (2013) 'Transcriptional control of cancer metastasis', *Trends in Cell Biology*.  
792 Elsevier Ltd, 23(12), pp. 603–611. doi: 10.1016/j.tcb.2013.06.001.
- 793 Farh, K. K.-H. *et al.* (2015) 'Genetic and epigenetic fine mapping of causal autoimmune disease  
794 variants.', *Nature*, 518(7539), pp. 337–43. doi: 10.1038/nature13835.
- 795 Femino, A. M. *et al.* (1998) 'Visualization of single RNA transcripts in situ.', *Science (New York,*  
796 *N.Y.)*, 280(5363), pp. 585–90. Available at: <http://www.ncbi.nlm.nih.gov/pubmed/9554849>.
- 797 Forrest, A. R. R. *et al.* (2014) 'A promoter-level mammalian expression atlas', *Nature*. Nature  
798 Publishing Group, 507(7493), pp. 462–470. doi: 10.1038/nature13182.
- 799 Harrow, J. *et al.* (2012) 'GENCODE: The reference human genome annotation for the ENCODE  
800 project', *Genome Research*, 22(9), pp. 1760–1774. doi: 10.1101/gr.135350.111.
- 801 Hayashi, T. *et al.* (2018) 'Single-cell full-length total RNA sequencing uncovers dynamics of  
802 recursive splicing and enhancer RNAs', *Nature Communications*. Springer US, 9(1), p. 619. doi:  
803 10.1038/s41467-018-02866-0.
- 804 Heldin, C. H., Vanlandewijck, M. and Moustakas, A. (2012) 'Regulation of EMT by TGF $\beta$  in  
805 cancer', *FEBS Letters*, 586(14), pp. 1959–1970. doi: 10.1016/j.febslet.2012.02.037.
- 806 Hon, C. C. *et al.* (2017) 'An atlas of human long non-coding RNAs with accurate 5' ends', *Nature*.  
807 Nature Publishing Group, 543(7644), pp. 199–204. doi: 10.1038/nature21374.
- 808 Ikushima, H. and Miyazono, K. (2010) 'TGF $\beta$  signalling: a complex web in cancer  
809 progression.', *Nature reviews. Cancer*. Nature Publishing Group, 10(6), pp. 415–24. doi:  
810 10.1038/nrc2853.
- 811 Islam, S. *et al.* (2014) 'Quantitative single-cell RNA-seq with unique molecular identifiers',  
812 *Nature Methods*, 11(2), pp. 163–166. doi: 10.1038/nmeth.2772.
- 813 Ji, Z. and Ji, H. (2016) 'TSCAN: Pseudo-time reconstruction and evaluation in single-cell RNA-  
814 seq analysis.', *Nucleic acids research*, 44(13), p. e117. doi: 10.1093/nar/gkw430.
- 815 Kiselev, V. Y. *et al.* (2017) 'SC3: consensus clustering of single-cell RNA-seq data.', *Nature*  
816 *methods*, 14(5), pp. 483–486. doi: 10.1038/nmeth.4236.
- 817 Lam, M. T. Y. *et al.* (2014) 'Enhancer RNAs and regulated transcriptional programs', *Trends in*  
818 *Biochemical Sciences*. Elsevier Ltd, 39(4), pp. 170–182. doi: 10.1016/j.tibs.2014.02.007.
- 819 Langfelder, P. and Horvath, S. (2008) 'WGCNA: An R package for weighted correlation network  
820 analysis', *BMC Bioinformatics*, 9(1), p. 559. doi: 10.1186/1471-2105-9-559.
- 821 Lassmann, T. (2015) 'TagDust2: a generic method to extract reads from sequencing data.',  
822 *BMC bioinformatics*, 16, p. 24. doi: 10.1186/s12859-015-0454-y.



- 823 Leng, N. *et al.* (2015) 'Oscope identifies oscillatory genes in unsynchronized single-cell RNA-  
824 seq experiments.', *Nature methods*, 12(10), pp. 947–950. doi: 10.1038/nmeth.3549.
- 825 Li, H. and Durbin, R. (2010) 'Fast and accurate long-read alignment with Burrows-Wheeler  
826 transform.', *Bioinformatics (Oxford, England)*, 26(5), pp. 589–95. doi:  
827 10.1093/bioinformatics/btp698.
- 828 Li, W., Notani, D. and Rosenfeld, M. G. (2016) 'Enhancers as non-coding RNA transcription  
829 units: Recent insights and future perspectives', *Nature Reviews Genetics*. Nature Publishing  
830 Group, 17(4), pp. 207–223. doi: 10.1038/nrg.2016.4.
- 831 Liberzon, A. *et al.* (2015) 'The Molecular Signatures Database (MSigDB) hallmark gene set  
832 collection.', *Cell systems*, 1(6), pp. 417–425. doi: 10.1016/j.cels.2015.12.004.
- 833 Liu, J. H. *et al.* (1999) 'Functional association of TGF- $\beta$  receptor II with cyclin B', *Oncogene*,  
834 18(1), pp. 269–275. doi: 10.1038/sj.onc.1202263.
- 835 Lun, A. T. L., Bach, K. and Marioni, J. C. (2016) 'Pooling across cells to normalize single-cell  
836 RNA sequencing data with many zero counts.', *Genome biology*, 17, p. 75. doi:  
837 10.1186/s13059-016-0947-7.
- 838 Lun, A. T. L., McCarthy, D. J. and Marioni, J. C. (2016) 'A step-by-step workflow for low-level  
839 analysis of single-cell RNA-seq data with Bioconductor', *F1000Research*, 5, p. 2122. doi:  
840 10.12688/f1000research.9501.2.
- 841 Massagué, J. (2008) 'TGF $\beta$  in Cancer', *Cell*, 134(2), pp. 215–230. doi:  
842 10.1016/j.cell.2008.07.001.
- 843 Mathelier, A. *et al.* (2016) 'JASPAR 2016: a major expansion and update of the open-access  
844 database of transcription factor binding profiles.', *Nucleic acids research*, 44(D1), pp. D110-5.  
845 doi: 10.1093/nar/gkv1176.
- 846 Moreb, J. S. *et al.* (2008) 'ALDH isozymes downregulation affects cell growth, cell motility and  
847 gene expression in lung cancer cells.', *Molecular cancer*, 7, p. 87. doi: 10.1186/1476-4598-7-87.
- 848 Mousavi, K. *et al.* (2013) 'eRNAs promote transcription by establishing chromatin accessibility at  
849 defined genomic loci.', *Molecular cell*. Elsevier Inc., 51(5), pp. 606–17. doi:  
850 10.1016/j.molcel.2013.07.022.
- 851 Munro, S. A. *et al.* (2014) 'Assessing technical performance in differential gene expression  
852 experiments with external spike-in RNA control ratio mixtures.', *Nature communications*, 5, p.  
853 5125. doi: 10.1038/ncomms6125.
- 854 Murata, M. *et al.* (2014) 'Detecting expressed genes using CAGE.', *Methods in molecular  
855 biology (Clifton, N.J.)*, 1164, pp. 67–85. doi: 10.1007/978-1-4939-0805-9\_7.
- 856 Picelli, S. (2017) 'Single-cell RNA-sequencing: The future of genome biology is now.', *RNA*



- 857 *biology*, 14(5), pp. 637–650. doi: 10.1080/15476286.2016.1201618.
- 858 Plessy, C. *et al.* (2010) 'Linking promoters to functional transcripts in small samples with  
859 nanoCAGE and CAGEscan', *Nature Methods*, 7(7), pp. 528–534. doi: 10.1038/nmeth.1470.
- 860 Poulain, S. *et al.* (2017) 'NanoCAGE: A method for the analysis of coding and noncoding 5'-  
861 capped transcriptomes', *Methods in Molecular Biology*, 1543, pp. 57–109. doi: 10.1007/978-1-  
862 4939-6716-2\_4.
- 863 Rahman, S. *et al.* (2016) 'Single-cell profiling reveals that eRNA accumulation at enhancer-  
864 promoter loops is not required to sustain transcription', *Nucleic Acids Research*, 45(6), pp.  
865 3017–3030. doi: 10.1093/nar/gkw1220.
- 866 Raj, A. *et al.* (2008) 'Imaging individual mRNA molecules using multiple singly labeled probes.',  
867 *Nature methods*, 5(10), pp. 877–9. doi: 10.1038/nmeth.1253.
- 868 Ramírez, F. *et al.* (2016) 'deepTools2: a next generation web server for deep-sequencing data  
869 analysis', *Nucleic Acids Research*, 44(W1), pp. W160–W165. doi: 10.1093/nar/gkw257.
- 870 Roadmap Epigenomics Consortium *et al.* (2015) 'Integrative analysis of 111 reference human  
871 epigenomes.', *Nature*, 518(7539), pp. 317–30. doi: 10.1038/nature14248.
- 872 Sadasivam, S. and DeCaprio, J. A. (2013) 'The DREAM complex: Master coordinator of cell  
873 cycle-dependent gene expression', *Nature Reviews Cancer*, 13(8), pp. 585–595. doi:  
874 10.1038/nrc3556.
- 875 Schneider, D., Tarantola, M. and Janshoff, A. (2011) 'Dynamics of TGF- $\beta$  induced epithelial-to-  
876 mesenchymal transition monitored by Electric Cell-Substrate Impedance Sensing', *Biochimica  
877 et Biophysica Acta - Molecular Cell Research*. Elsevier B.V., 1813(12), pp. 2099–2107. doi:  
878 10.1016/j.bbamcr.2011.07.016.
- 879 Scialdone, A. *et al.* (2015) 'Computational assignment of cell-cycle stage from single-cell  
880 transcriptome data.', *Methods (San Diego, Calif.)*, 85, pp. 54–61. doi:  
881 10.1016/j.ymeth.2015.06.021.
- 882 Shibayama, Y., Fanucchi, S. and Mhlanga, M. M. (2017) 'Visualization of enhancer-derived  
883 noncoding RNA', *Methods in Molecular Biology*, 1468, pp. 19–32. doi: 10.1007/978-1-4939-  
884 4035-6\_3.
- 885 Shiraki, T. *et al.* (2003) 'Cap analysis gene expression for high-throughput analysis of  
886 transcriptional starting point and identification of promoter usage', *Proceedings of the National  
887 Academy of Sciences*, 100(26), pp. 15776–15781. doi: 10.1073/pnas.2136655100.
- 888 Suter, D. M. *et al.* (2011) 'Mammalian genes are transcribed with widely different bursting  
889 kinetics.', *Science (New York, N.Y.)*, 332(6028), pp. 472–4. doi: 10.1126/science.1198817.
- 890 Svensson, V. *et al.* (2017) 'Power analysis of single-cell RNA-sequencing experiments.', *Nature*

- 891 *methods*. Nature Publishing Group, 14(4), pp. 381–387. doi: 10.1038/nmeth.4220.
- 892 Tang, D. T. P. *et al.* (2013) ‘Suppression of artifacts and barcode bias in high-throughput  
893 transcriptome analyses utilizing template switching’, *Nucleic Acids Research*, 41(3), p. e44. doi:  
894 10.1093/nar/gks1128.
- 895 Trapnell, C. (2015) ‘Defining cell types and states with single-cell genomics’, *Genome Research*,  
896 25(10), pp. 1491–1498. doi: 10.1101/gr.190595.115.
- 897 Tung, P.-Y. *et al.* (2017) ‘Batch effects and the effective design of single-cell gene expression  
898 studies.’, *Scientific reports*. Nature Publishing Group, 7(January), p. 39921. doi:  
899 10.1038/srep39921.
- 900 Wagner, A., Regev, A. and Yosef, N. (2016) ‘Revealing the vectors of cellular identity with  
901 single-cell genomics’, *Nature Biotechnology*. Nature Publishing Group, 34(11), pp. 1145–1160.  
902 doi: 10.1038/nbt.3711.
- 903 Williams, C. M. J. *et al.* (2009) ‘AP-2 $\gamma$  promotes proliferation in breast tumour cells by direct  
904 repression of the CDKN1A gene’, *The EMBO Journal*. Nature Publishing Group, 28(22), pp.  
905 3591–3601. doi: 10.1038/emboj.2009.290.
- 906 Wong, P.-P. *et al.* (2012) ‘Histone Demethylase KDM5B Collaborates with TFAP2C and Myc To  
907 Repress the Cell Cycle Inhibitor p21<sup>cip</sup> (CDKN1A)’, *Molecular and Cellular Biology*, 32(9), pp.  
908 1633–1644. doi: 10.1128/MCB.06373-11.
- 909 Wu, A. R. *et al.* (2014) ‘Quantitative assessment of single-cell RNA-sequencing methods.’,  
910 *Nature methods*, 11(1), pp. 41–6. doi: 10.1038/nmeth.2694.
- 911 Wu, D. and Smyth, G. K. (2012) ‘Camera: a competitive gene set test accounting for inter-gene  
912 correlation.’, *Nucleic acids research*, 40(17), p. e133. doi: 10.1093/nar/gks461.
- 913 Young, M. D. *et al.* (2010) ‘Gene ontology analysis for RNA-seq: accounting for selection bias.’,  
914 *Genome biology*, 11(2), p. R14. doi: 10.1186/gb-2010-11-2-r14.